UHASSELT
KNOWLEDGE IN ACTION

Maastricht University

Faculty of Medicine and Life Sciences
School for Life Sciences
Master of Biomedical Sciences

Master's thesis

Multi-model evaluation of suicide gene therapy with human dental pulp stem cells for oral squamous cell carcinoma

Thomas Raps

Thesis presented in fulfillment of the requirements for the degree of Master of Biomedical Sciences, specialization Molecular Mechanisms in Health and Disease

SUPERVISOR :

Prof. dr. Esther WOLFS

MENTOR :

Mevrouw Jolien VAN DEN BOSCH

2023
2024

Transnational University Limburg is a unique collaboration of two universities in two countries: the University of Hasselt and Maastricht University.

UHASSELT
KNOWLEDGE IN ACTION

www.uhasselt.be
Universiteit Hasselt
Campus Hasselt:
Martelarenlaan 42 | 3500 Hasselt
Campus Diepenbeek:
Agoralaan Gebouw D | 3590 Diepenbeek

Faculty of Medicine and Life Sciences
School for Life Sciences
Master of Biomedical Sciences

Master's thesis

Multi-model evaluation of suicide gene therapy with human dental pulp stem cells for oral squamous cell carcinoma

Thomas Raps

Thesis presented in fulfillment of the requirements for the degree of Master of Biomedical Sciences, specialization Molecular Mechanisms in Health and Disease

SUPERVISOR :

Prof. dr. Esther WOLFS

MENTOR :

Mevrouw Jolien VAN DEN BOSCH

Multi-model evaluation of suicide gene therapy with human dental pulp stem cells for oral squamous cell carcinoma*

Thomas Raps[1], Jolien Van den Bosch[1] and Esther Wolfs[1]

[1]UHasselt – Hasselt University, Functional Imaging & Research on Stem Cells (FIERCE) lab, Biomedical Research Institute, Agoralaan Gebouw C - B-3590 Diepenbeek

*Running title: *Suicide gene therapy with hDPSC for OSCC*

To whom correspondence should be addressed: Esther Wolfs, Tel: +32 11 26 92 96; Email: esther.wolfs@uhasselt.be

Keywords: Gap Junctional intercellular Communication (GJIC), Herpes Simplex Virus type 1 Thymidine Kinase (HSV1-TK), human Dental Pulp Stem Cells (hDPSC), Oral Squamous Cell Carcinoma (OSCC), Suicide Gene Therapy

ABSTRACT

Oral squamous cell carcinoma (OSCC) is the most prevalent head and neck cancer. Current treatments do not significantly improve the patient's survival rate and are associated with severe side effects. Hence, a more local and targeted strategy is acquired to enhance the therapeutic efficacy and the patient's quality of life. In this project, a suicide gene therapy based on the herpes simplex virus type 1 – thymidine kinase/ganciclovir (HSV1-TK/GCV) system will be examined. Human dental pulp stem cells (hDPSC) will be utilized as an HSV1-TK carrier *in vitro*. This enables the cells to convert GCV into its cytotoxic form. Through gap junctions, the cytotoxic GCV will induce OSCC apoptosis. The strategy's efficacy was evaluated in co-cultures of HSV1-TK$^+$-hDPSC and OSCC. The killing efficiency after GCV administration was examined using an alamarBlue analysis. Here, a cell viability reduction was established with GCV concentrations starting from 10 µM and 600 µM in 2D and 3D co-cultures, respectively. Additionally, xenograft mice containing HSV1-TK$^+$-OSCC cells were assessed with BLI. Moreover, additional cancer types were examined to expand the proposed therapy to various tumors. After GCV administration for 19-25 consecutive days, there was a significant decrease in photon emission in OSCC, breast, colon, kidney, pancreatic, lung, and skin cancer, indicating cell death. Furthermore, gap junctions were identified by connexin 43 immunocytochemistry in breast, colon, kidney, pancreatic, and lung cancer. In summary, our findings demonstrate the potential of HSV1-TK$^+$-hDPSC as a novel targeted strategy for OSCC and the potential expansion of this therapy to other cancers.

INTRODUCTION

Cancer – **Cancer**, also referred to as neoplasm or malignant tumor, ranks as the second leading cause of death worldwide. This diverse group of diseases can originate in any tissue or organ within the body and is characterized by the unregulated proliferation of cells that can invade neighboring tissues via a process called metastasis. Potential risk factors for developing these malignancies are air pollution, alcohol consumption, chronic infections, lack of physical activity, tobacco use, and unhealthy diets (1). Cancer is a complex disease that is characterized by ten hallmarks, including the ability to evade growth suppressors, activation invasion and metastasis, avoid immune destruction, deregulate cellular metabolism, enable replicative immortality, genome mutations and instability, induce or acquire vasculature, sustain proliferative signaling, tumor-promoting inflammation, and withstand cell death (2). These hallmarks are crucial in understanding cancer and the development of effective treatments.

Head and neck cancer – Head and neck squamous cell carcinomas (HNSCC) rank as the seventh most prevalent cancer type worldwide. According to the latest Global Cancer

Observatory (GLOBOCAN), the annual incidence and mortality of HNSCC are 890.000 and 450.000, respectively (3). The most common subtype of HNSCC is **oral squamous cell carcinoma** (OSCC), which accounts for over 50% of HNSCC cases (4). OSCC manifests in the oral cavity and oropharynx due to genetic mutation accumulations and is often associated with chewing of areca nut, inadequate nutrition, poor oral hygiene, and infections of the human papillomavirus (HPV) and the Epstein-Barr virus. However, the most significant risk factors remain alcohol consumption and tobacco use. Due to a late diagnosis, the 5-year survival rate of OSCC persists at a mere 30-50% (5, 6). In addition, conventional treatments, including chemotherapy, immunotherapy, radiotherapy, surgery, and combinatorial therapy, do not reduce mortality (4, 5). Moreover, these systemic therapies often result in limited therapeutic efficacy and the development of drug resistance. These treatments frequently induce functional impairment in the surrounding healthy tissues, leading to adverse effects (7-9). For instance, chemotherapy may lead to constipation, fatigue, hair loss, increased risk of infections, and mouth ulcers (10). Additionally, surgery may cause issues with chewing, speech, and swallowing and could lead to neurologic injuries (11). Consequently, these approaches often lead to anxiety, emotional disturbance, and pain, adversely impacting the quality of life for patients (9). Hence, a more local and targeted strategy is necessary to minimize these effects caused by the current systemic treatments.

Gene therapy – Compared to conventional treatments, gene therapy is a more specific and **targeted strategy** for cancer treatment. Gene therapy is divided into various subtypes, namely (i) corrective, (ii) toxin/apoptosis-inducing, and (iii) suicide gene therapy. Initially, corrective gene therapy targets aberrant genetic elements to impede the proliferation of cancer cells. Genetic interference agents, such as miRNA, which disrupt the proliferation cycle, and tumor suppressor genes like *p53* are commonly utilized examples. Secondly, toxin/apoptosis-inducing gene therapy utilizes transgenes – foreign genes introduced into cells – to produce toxic proteins, such as diphtheria toxin or TNF-α, ultimately triggering apoptosis. However, only the cells that receive the therapeutic agent are affected, which is a limitation of both methods as other cells will continue to proliferate. The last subtype, suicide gene therapy, overcomes this disadvantage (12).

Suicide gene therapy – Gene-directed enzyme prodrug therapy (GDEPT), or suicide gene therapy, is a treatment strategy that involves three components: a carrier, a prodrug, and a genetically engineered enzyme. The enzyme is responsible for catalyzing the conversion of the prodrug into its active form, which causes cell cycle arrest, leading to apoptosis (13). One of the most extensively studied GDEPT in cancer treatment are **the herpes simplex virus type I - thymidine kinase** (HSV1-TK) with ganciclovir (GCV) and the cytosine deaminase (CD) with 5-fluorocytosine (5-FC) systems (14). The latter utilizes the prodrug 5-FC, which CD converts to its toxic form of 5-fluorouracil (5-FU). Consequently, the cytotoxic pathways will lead to 5-FU RNA, DNA complexes, and the inhibition of thymidylate synthase, ultimately inducing cell apoptosis (13, 14). However, clinical success is limited due to the short half-life, poor selectivity, and drug resistance of 5-FU (13, 15). Furthermore, the cytotoxic compounds are non-specific, affecting healthy cells and leading to side effects (15).

Herpes simplex virus type I - thymidine kinase/ganciclovir system – The most utilized suicide gene therapy is the HSV1-TK/GCV system, where cells contain the *HSV1-tk* gene. Hence, an HSV1-TK enzyme is produced, which converts the administered non-toxic prodrug GCV into GCV mono-phosphate (GCV-1P). Subsequently, cellular TK phosphorylates GCV-1P into its **cytotoxic triphosphate form** (GCV-3P), which is an analog of 2'-deoxyguanosine triphosphate (dGTP), leading to DNA polymerase inhibition and the integration into replicating DNA (12, 13, 16). Finally, GCV-3P leads to cell apoptosis via double-strand breaks and cell cycle arrests (17). The selectivity of this strategy is enhanced by the affinity of the HSV1-TK enzyme, which is a thousand times higher than the cytosolic TK (12). Furthermore, the affinity of GCV is influenced by the choice of TK subtype. The TK mutants sr11 and sr26 exhibit a 7.4- and 2.7-fold affinity increase, respectively, compared to wild-type TK. Notably, sr39 displays the highest affinity, demonstrating a remarkable 14.3-fold increase (18). Moreover, sr39 reduces the dose of prodrug needed by 294-fold, drastically diminishing the non-specific toxicity

(12). Furthermore, HSV1-sr39TK shows promise as a reporter gene in positron emission tomography (PET). Accumulation of radioactive-labeled GCV is increased by 2.0-fold when HSV1-sr39TK is utilized compared to wild-type HSV1-TK. Consequently, the application of the **sr39-variant** in suicide gene therapy holds great potential (19). Furthermore, the HSV1-TK/GCV system incorporates a safety mechanism, ensuring that genetically modified cells undergo cell death upon GCV administration (20, 21). However, before the initiation of the safety switch, the manipulated cells transfer the toxic GCV to neighboring cells, indirectly inducing apoptosis – a phenomenon known as **the bystander effect** (12, 18).

The bystander effect – The therapeutic effects of GDEPT are dependent on the bystander effect, which can be divided into three types: (i) Endocytosis, (ii) the distant bystander effect, and (iii) gap junctional intercellular communication (GJIC). In the first category, transduced cells release apoptotic bodies that induce apoptosis in unmodified adjacent cells by endocytosis. The second mechanism involves the activation of the immune system, as various immune cells are drawn to the tumor site. Subsequently, the systemic immune response initiates at metastatic sites, potentially preventing secondary tumor formations. The third phenomenon utilizes active transport via **gap junctional intercellular communication** (**Figure 1)** (12). These gap junctions enable the transfer of GCV-3P between adjacent HSV1-TK positive and negative cells, as the highly charged GCV-3P cannot diffuse through the cell membrane (13). GJIC occurs when gap junctions connect, which consist of two connexons, each composed of six connexins. The most common connexin in human cells is connexin 43 (Cx43), one of the most extensively studied connexin subtypes (22). Hence, Cx43 is an essential indicator for investigating GJIC (23). However, as mentioned above, a carrier is necessary to deliver *HSV1-tk* to the target site to achieve the desired bystander effect. The delivery is categorized into (i) viral, (ii) non-viral, and (iii) cell-based systems (24). The most utilized types in GDEPT are viral vectors, specifically those originating from adenoviruses (AdV), adeno-associated viruses (AAV), and lentiviruses. AdV provide high transduction efficiency in non- and dividing cells, and they do not integrate into the host genome, lowering the risk of insertional mutagenesis. However, the latter limits long-term expression. Furthermore, AdV initiate a robust immune response, leading to undesirable effects (25). Conversely, AAV have shown less immunogenic responses. Nevertheless, AAV are limited in packaging capacity (max. of 4kB foreign DNA) (26, 27). In contrast to AdV and AAV, lentiviral vectors integrate into the host genome, preserving long-term expression. Furthermore, these vectors are capable of expressing multiple genes. However, a notable drawback is the increased risk of insertional mutagenesis (25, 28). In general, the complexity, high production costs, and safety concerns make this a suboptimal strategy in clinical applications (27). Compared to viral vectors, non-viral delivery systems have increased safety, lower immunogenicity, and ease of performance (29). Physical methods, such as electroporation and microinjection, are commonly used to introduce genetic materials through cell membranes. Furthermore, chemical vectors, such as liposomes and polymers, deliver the additional genes by endocytosis into the cells (30). Nevertheless, non-viral delivery systems are limited due to poor gene transfer efficiency (24). Lastly, **cell-based delivery** involves the administration of living cells carrying a suicide gene (31). This targeted delivery system provides increased efficacy, precision, safety, and sustainability (32). A promising cell type for inducing a suicide gene, such as *HSV1-tk*, is mesenchymal stem cells (MSC) (33).

Mesenchymal stem cells – MSC are plastic adherent and can differentiate into adipogenic, chondrogenic, and osteogenic lineages *in vitro*. Furthermore, over 95% of the MSC population expresses the surface markers CD73, CD90, and CD105 and lacks the expression of CD11b, CD14, CD19, CD34, CD45, and CD79α. MSC have a homing capacity toward injured tissue and tumor sites (34). Additionally, these stem cells contain immunomodulatory capacities, allowing them to avoid the host's immune system (35). One subtype of MSC, namely **human dental pulp stem cells** (hDPSC), has an additional advantage compared to other MSC: the simplicity of isolation. hDPSC are harvested from third molars (wisdom teeth), a relatively easy and low-invasive procedure (36, 37). Furthermore, wisdom teeth are a universal source of stem cells as they are considered

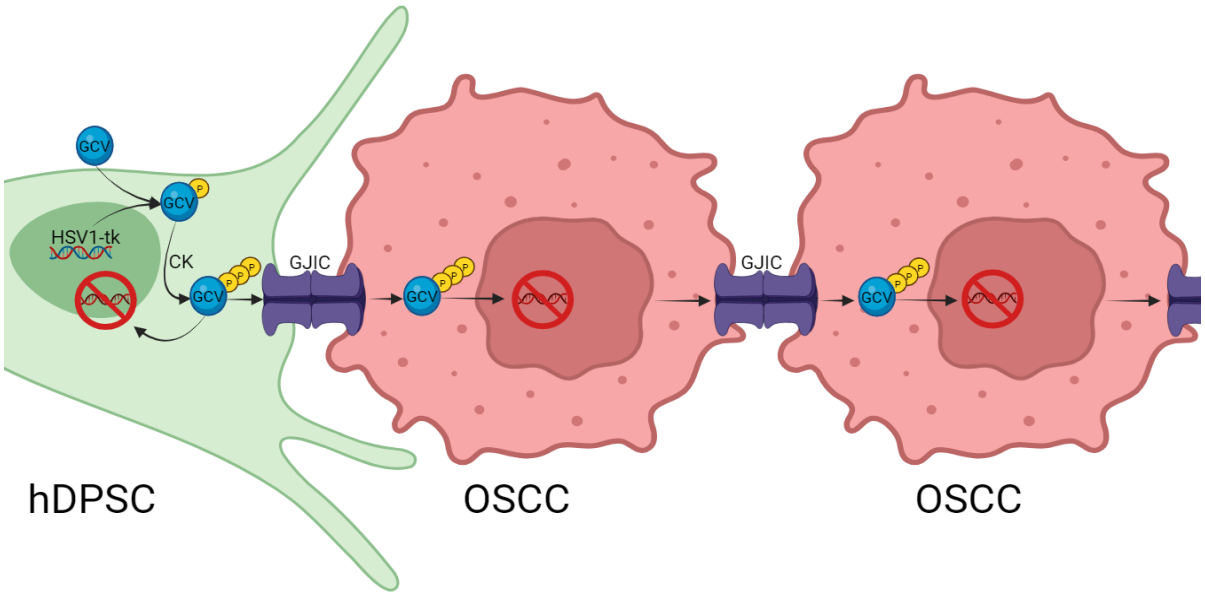

Figure 1 - A graphical overview of the bystander effect utilizing the HSV-TK/GCV system for OSCC. Human dental pulp stem cells (hDPSC) are transduced with a lentiviral vector containing the herpes simplex virus type I thymidine kinase (*HSV1-tk*) gene. Administered ganciclovir (GCV) can diffuse through the cell membrane of the hDPSC. Consequently, the HSV1-TK enzyme will phosphorylate GCV. Next, cellular kinases (CK) will form the cytotoxic triphosphate form of GCV (GCV-3P). Preliminary data has shown that the hDPSC form functional gap junctions with the oral squamous carcinoma (OSCC) cells. GVC-3P enters the nucleus and integrates into the DNA, ultimately inducing apoptosis of both cell types. Figure made in BioRender. *GJIC, gap junctional intercellular communication.*

waste products (38). Consequently, hDPSC are promising as a carrier for suicide gene therapy (36). Foremost, the HSV1-TK/GCV system utilizing hDPSC needs to be validated.

Imaging methods – Cell-based delivery of suicide gene therapy, for example via hDPSC, can be validated through three commonly utilized non-invasive imaging techniques: (i) bioluminescence imaging (BLI), (ii) magnetic resonance imaging (MRI), and (iii) PET. These methods can evaluate the survival of genetically modified stem cells and tumor cells, providing insights into the therapy's efficacy (36, 39, 40). First, BLI can be utilized when the genetically modified cells contain an additional *Firefly Luciferase (Fluc)* gene. Administered luciferin is oxidated by luciferase inside living cells, which results in detectable emission light (530-640 nm) (36, 39). Second, MRI and PET are commonly utilized for measuring tumor volume (40). MRI constructs detailed images by changing the magnetic vector of hydrogen nuclei distributed in tissues. Initially, all vectors are randomly aligned. However, by utilizing a magnetic field, the hydrogen atoms of water molecules align throughout the body. After a transient perturbation by radiofrequency pulses, the magnetic dipoles will return to their basic aligned state while emitting electromagnetic waves that the scanner can detect, creating detailed images (41). Besides morphology, tumor metabolism is another captivating factor that can be investigated using PET. Hereby, PET scans will rely on ^{18}F-labeled-fluoro-2-deoxyglucose (^{18}F-FDG), a radioactive glucose analog that accumulates in tissue with high glucose metabolism, such as tumors, after being injected into the bloodstream (42, 43). Moreover, ^{18}F-FDG interacts with a free electron, resulting in an emission signal of two photons in opposite directions (44). Consequently, the viability of the tumor is measured (43).

Experimental approach – In this study, lentivirally transduced hDPSC containing *HSV1-tk* will be utilized as a carrier in suicide gene therapy in combination with the non-toxic prodrug GCV. Due to GJIC, the toxic compound is transferred into the neighboring OSCC cells, inducing apoptosis at the tumor site. Consequently, hDPSC will be highlighted as a promising novel source capable of reducing OSCC tumor growth by suicide gene therapy. Hence, the study focuses on a new, local, and targeted treatment, diminishing the side effects caused by the current systemic therapies. The

hypothesis indicates that the HSV1-TK/GCV system is an efficient strategy against OSCC by inducing apoptosis of the tumor cells caused by the bystander effect. The efficacy of the HSV1-TK/GCV system will be validated by examining tumor cell apoptosis *in vitro* and *in vivo*. First, 2D and 3D hDPSC-OSCC co-cultures will be established. However, considering the clinical relevance, various ratios with less hDPSC than OSCC cells will be investigated in the 2D co-cultures. The 3D model will add relevance to our *in vitro* research by using a collagen-based hydrogel, which shares similarities with the *in vivo* extracellular matrix (ECM) (45). Both co-cultures will be exposed to various GCV concentrations. Second, as a proof-of-concept, an immunodeficient xenograft mouse model will be utilized to mitigate any potential interference from the immune system. After subcutaneous injection of HSV1-TK$^+$-OSCC cells, GCV will be intraperitoneally injected. BLI will evaluate tumor growth. Lastly, various cancer types will be included to assess the therapy's potential to expand to other tumors beyond OSCC.

Various experiments were conducted prior to this study to successfully perform and validate our current research results. In the context of the HSV1-TK/GCV system, GJIC forms the foundation of our project. Consequently, immunostainings of Cx43 were performed to visualize the gap junction formation between OSCC cells. Furthermore, these connexins were also observed in 2D and 3D co-cultures of hDPSC and OSCC cells. In addition, a single-cell microinjection assay of hDPSC with impermeable lucifer yellow dye was used to evaluate gap junction functionality where the diffusion of this dye to adjacent cells was observed. Additionally, GJIC was blocked with Cx43shRNA to inhibit the diffusion of the injected dye to adjacent cells.

EXPERIMENTAL PROCEDURES

Cell isolation and culturing – hDPSC were isolated from wisdom teeth, which were collected from healthy individuals during tooth extractions for orthodontic or therapeutic reasons in the hospital 'Ziekenhuis Oost-Limburg' (ZOL, Genk, Belgium). The isolation method was previously described by Hilkens *et al*. (37). The hDPSC were cultured in Alpha Minimum Essential Medium (α-MEM) (Capricorn scientific, MEMA-XRXA), supplemented with 10% Fetal Calf Serum (FCS) (Biowest, S00FL10D01), 2 mM L-glutamine (G7513, Sigma-Aldrich), 1% penicillin-streptomycin (Gibco, 15140-122) at 37°C and 5% CO_2. The culture medium was refreshed every 2 to 3 days.

The UM-SCC-14C tumor cell line (CVCL_7721, Cell Lines Service (CLS), Eppelheim, Germany) of human OSCC cells was cultured in Dulbecco's Modified Eagle Medium/Nutrient Mixture F-12 (DMEM/F-12) (Gibco, 11330-032), enriched with 5% Fetal Calf Serum, 2 mM L-glutamine, 1% penicillin-streptomycin at 37°C and 5% CO_2.

The additional mouse cell lines B16F10 (CRL-1642), EMT-6 (CRL-2755), HEPA1-6 (CRL-1830) LL2 (CRL-1642), MC38 (abm TB291), PAN02 (IOC-ZP322), and RENCA cells (400321) were utilized. The Roswell Park Memorial Institute (RMPI) medium (Gibco, 22400-089) was utilized for the RENCA cells. The other cell types were cultured in DMEM (Gibco, 41965-062). All media were enriched with 10% FCS and 1% penicillin-streptomycin.

HSV1-TK transduction – hDPSC, humane OSCC cell line, and murine tumor cell lines B16F10, EMT-6, HEPA1-6, LL2, MC38, PAN02, and RENCA were transduced with a lentiviral vector (generated by the protocol of Tiscornia *et al*. (28)) encoding an Elongation Factor 1 Alpha (EF1α) promotor, *HSV1-sr39tk*, T2A sequence, *FLuc*, Flag-tag, His-tag, Internal Ribosome Entry Site (IRES) sequence, and *Puromycin Resistance (PuroR)*. The obtained lentiviral particles were added to the different cell cultures. The transduced cells were selected by the administration of 2 µg/mL puromycin (#ant-pr-1, InvivoGen) for 3 days.

Cell co-culturing – The 2D and 3D hDPSC-OSCC co-cultures were constructed with HSV1-TK$^+$-hDPSC and OSCC. The ratios used for the 2D co-cultures were 1:1, 1:5, and 1:10. In contrast, the 3D co-cultures were constructed in a ratio of 1:1. Furthermore, the 3D co-cultures were made in a collagen-hydrogel, which were formed out of 10.000 cells/µl mixed with 10% Minimum Essential Medium Eagle (MEM) (Sigma-Aldrich, M4526) and 80% type 1 rat tail collagen (First Link, Wolverhampton) (5 mg/ml in 0.6% acetic acid), followed by neutralization with sodium hydroxide.

Cell viability assays of 2D and 3D HSV1-TK$^+$-hDPSC-OSCC co-cultures – The experimental procedure was initiated after the co-cultures achieved approximately 100%

confluence. The 2D co-cultures were exposed to 0, 0.1, 1, 10, 100, and 1000 µM GCV, while the initial 3D model also included 0.01 µM GCV. GCV administrations to the 2D and 3D models were conducted every 2 to 3 days for 7 and 14 days, respectively. Furthermore, 0, 10, 100, 300, 600, 800, and 1000 µM GCV was utilized every 2 to 3 days for the alternative 3D co-cultures for 14 days. The alamarBlue assay (Invitrogen, Thermo Fisher Scientific, BUF012B) was performed according to the manufacturer's instructions. In brief, alamarBlue was added in a 1/10 ratio and incubated for 3 to 4 hours. The fluorescence (540-590 nm) was measured with the CLARIOstar PLUS plate reader (BMGLABTECH, De Meern, The Netherlands).

Immunocytochemistry – $3{,}5x10^4$ cells/cm^2 B16F10, EMT-6, HEPA1-6, LL2, MC38, PAN02, and RENCA cells were seeded on glass coverslips in a 24-well plate. After achieving 80-90% confluency, cells were fixed with 4% paraformaldehyde (PFA) in 1x phosphate-buffered saline (PBS) (VWR, VWRMS01VH) for 20 minutes. The cells were incubated in a 10% protein block (Dako, X090) in 1x PBS for 1 hour to prevent non-specific bindings. Subsequently, the anti-Cx43 primary antibody (Abcam, Cambridge, United Kingdom, 1/1000) was incubated overnight at 4°C. The next day, Goat anti-Rabbit IgG (H+L) secondary antibody Alexa Fluor™ 555 (Invitrogen, Thermo Fisher Scientific, Geel, Belgium, 1/400) was added and incubated for approximately 2 hours, followed by nuclear counterstaining with 4,6-diamidino-2-phenylindole (DAPI 1/10.000, Boehringer Mannheim GmbH, Germany). Coverslips were mounted with Immu-mount (Thermofisher, 9990402), and pictures were taken at a 40x magnification with the Leica DM4000 B microscope (Leica Microsystems, Wetzlar, Germany). Images were processed by the FIJI ImageJ2 software.

In vivo bioluminescence imaging and tumor size assessment – Hsd:Athymic-Foxn1nu mice (Envigo, Horst, The Netherlands) were subcutaneously injected with the following HSV1-TK^+-cancer cells: $5x10^5$ B16F10, $5x10^5$ EMT6, $5x10^6$ HEPA1-6, $5x10^5$ LL2, $1x10^6$ MC38, $5x10^5$ OSCC, $5x10^6$ PAN02, or $5x10^5$ RENCA, resuspended in 50 µL DMEM medium with 50 µL growth factor-reduced Matrigel (Corning, Lasne, Belgium). The tumor size was measured by a caliper. After the tumors had an appropriate size, the treatment was initiated. The mice in the treatment and control group received daily intraperitoneal injections of 50 mg/kg GCV or an equivalent amount of PBS, respectively. The GCV was administered for 19 days for the mice with LL2 and RENCA cell lines. Mice containing PAN02 received GCV for 25 days. The assessment period for other tumors was over 21 days. Twice or thrice a week, the viability of the HSV1-TK^+-cancer cells was evaluated through BLI after subcutaneously administering 126 mg/kg D-luciferin (Promega, Leiden, The Netherlands). During the injections and the BLI measurement, the animals were anesthetized with isoflurane (2% in 100% oxygen at a flow rate of 2 L/min). Photon emission was measured where consecutive frames were received using IVIS lumina III (Perkin Elmer, Mechelen, Belgium) until maximum signal intensity was achieved. Regions of interest (ROI) were marked, and the total photon flux of the ROI was quantified. Mice were euthanized by cervical dislocation when humane endpoints were reached or at the end of the study.

Statistical analysis – All statistical analyses were performed using GraphPad Prism 10. The Shapiro-Wilk test evaluated the normal distribution of each data. Data that did not pass the normality test were transformed with a log or sqrt transformation. Following, the One-way ANOVA with Dunnett's multiple comparisons test or Two-way ANOVA was used. The significance level was set at $p < 0.05$. Furthermore, outliers were identified and excluded via the Robust Regression and Outlier Removal (ROUT) test with a Q-value of 1%. Data were represented as mean ± SEM.

RESULTS

In this study, we aimed to evaluate the therapeutic efficacy of the HSV1-TK/GCV system using HSV1-TK^+-hDPSC for OSCC. Our laboratory conducted extensive experiments before this paper to achieve this goal. Furthermore, the therapeutic hDPSC are developed and validated. Stem cell integrity and *HSV1-tk* expression were confirmed. In addition, hDPSC of various patients were utilized throughout this study. Based on our current findings, as mentioned previously, further research is needed on the mechanism's therapeutic efficacy.

Validation of the HSV1-TK/GCV system in 2D and 3D HSV1-TK$^+$-hDPSC-OSCC co-cultures – As previously mentioned, the suicide gene therapy system relies on GJIC between the cancer and stem cells. Hypothetically, the cytotoxic GCV will transit from the hDPSC to the OSCC cells and induce OSCC apoptosis. This mechanism was first examined by assessing the cell viability utilizing five and six different GCV concentrations in 2D and 3D hDPSC-OSCC co-cultures, respectively (**Figure 2**). The 2D co-cultures resulted in a significant reduction in cell viability from 10 µM to 1000 µM GCV. No significant results were observed in the 3D co-cultures, except for the administrations of 1000 µM GCV. Moreover, the cell viability decreased by 4% with 100 µM GCV and 92.22% with 1000 µM GCV.

Based on these outcomes, five GCV concentrations were applied to various ratios (1:1, 1:5, and 1:10) of hDPSC-OSCC in 2D co-cultures. The 3D model was exposed to six different GCV concentrations, between 10 µM and 1000 µM (**Figure 3**). The negative control group was treated with milli-Q (MQ), resulting in nearly complete cell death. 2D and 3D co-culture results indicated a significant concentration-dependent decrease in cell viability. Moreover, the 1:1 2D co-cultures showed reduced cell viability from 100 µM GCV. However, no significant results were obtained at the 1:5 and 1:10 ratios, except with the 1000 µM GCV administrations. The cells of the 3D model had a significant reduction at 600 µM, 800 µM, and 1000 µM GCV administration, which had an average cell viability of 58%, 52%, and 37%, respectively.

In vivo assessment of HSV1-TK$^+$-OSCC reduction in a xenograft mouse model.– HSV1-TK$^+$-OSCC cells were assessed *in vivo* after GCV or PBS treatment through BLI. Due to the presence of *FLuc* in the tumor cells, the emission of light photons directly correlates with the amount of viable tumor cells present. BLI measurements were acquired over 21 days, and a significant reduction in OSCC viability in the treatment group was observed from day 10 to day 17 (**Figure 4A**). No significance could be determined on day 21 after a log transformation because of the corresponding cancer cell viability of 0%. Representative images from days 0, 7, 14, and 21 of two mice were included, demonstrating a declining signal in the mouse receiving GCV and an escalating signal in the control mouse (**Figure 4B**). No image was obtained from the mice receiving GCV on day 21 due to the absence of a bioluminescence signal.

Cx43 membrane expression in various cancer cell lines – As described before, the efficacy of the HSV1-TK/GCV system is based on gap junction formations. To determine the potential of HSV1-TK/GCV therapy in tumors other than OSCC, further research is needed to examine the presence of these communication channels. Therefore, various cancer cell lines were utilized to investigate the presence of gap junctions through Cx43 immunocytochemical (ICC) staining. Cx43 (purple dots) was observed on the cell membrane in the EMT-6 (**Figure 5A**), LL2 (**Figure 5B**), MC38 (**Figure 5C**), PAN02 (**Figure 5D**), and RENCA (**Figure 5E**) cell lines. The cell lines of breast, pancreatic, and kidney cancer exhibited the highest levels of visible Cx43.

In vivo assessment of the HSV1-TK/GCV system in various cancer types – To determine the potential applicability of the therapy to other tumor types, a comprehensive proof-of-concept assessment is required. Various tumor types were utilized to evaluate cell death *in vivo* after daily GCV administrations. Different cancer cell lines were transduced with the *HSV1-tk* and *FLuc* genes and subcutaneously injected into mice. After luciferin administration, BLI was utilized to measure the emission of light photons, directly correlating with the amount of viable tumor cells present. BLI measurements were acquired over a time period of 19, 21, or 25 days, depending on the type of cell line.

The cell viability of both B16F10 and EMT6 was significantly reduced in the treatment group after three days (**Figure 6A & B**). The latter showed a significant difference in survival ($p < 0.0001$) between the control and treatment groups. By day 21, the viability of EMT6 cells in the treatment group was reduced to 0%. In contrast, the EMT6 tumors of the control mice reached the maximum permitted volume between the first and second week. Furthermore, B16F10 demonstrated a significant difference in survival ($p < 0.05$). However, even though the BLI signal decreased in the B16F10 treatment group, all mice were sacrificed due to an increased tumor volume according to caliper measurements.

The cell viability of the LL2 tumors was significantly reduced after GCV administrations, with an average cancer cell

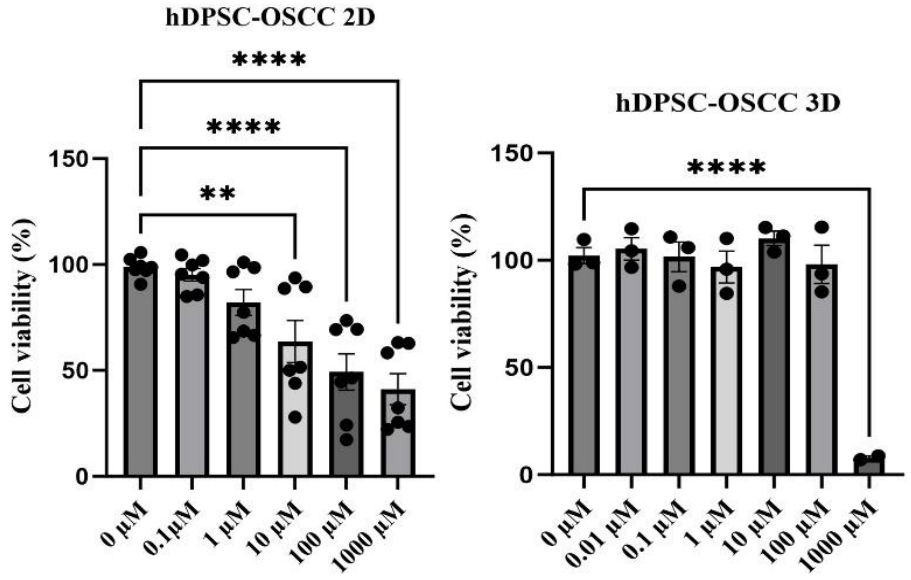

Figure 2 - Cell viability assessment of 2D and 3D HSV1-TK⁺-hDPSC-OSCC co-cultures after GCV administrations. 2D (n=7) and 3D (n=3) co-cultures were treated every 2 to 3 days with five and six different GCV concentrations, respectively, ranging from 0.01 µM to 1000 µM. The alamarBlue assay was performed after 7 and 14 days for the 2D and 3D co-cultures, respectively. A significant reduction was observed from 10 µM in the 2D culture. However, the 3D culture showed only a significant reduction in cell viability from 1000 µM. Each data is expressed as mean ± SEM. Data were normally distributed. One outlier was detected and removed from the 3D model. One-way ANOVA with Dunnett's multiple comparisons test was used. *$p \leq 0.05$, **$p \leq 0.01$, ****$p \leq 0.0001$. *hDPSC, human Dental Pulp Stem Cells; OSCC, Oral Squamous Cell Carcinoma.*

viability of 0.62% on day 19 (**Figure 6C**). Moreover, the treatment group showed weak or absent bioluminescence signals on day 12 and increased survival compared to the control group.

Between the two mice groups of MC38, significant differences were observed only on days 3 and 7 due to missing data (**Figure 6D**). The exclusion of several control mice led to the cessation of data collection from mice receiving PBS after day 7, as the remaining control animals had reached the humane endpoint. Nevertheless, the treatment mice containing MC38 tumors showed no bioluminescent signal on day 21 and showed improved survival ($p < 0.0001$).

A significant difference was measured in the RENCA cell line on days 11 and 16 (**Figure 6E**). On day 19, a cancer cell viability of 0% was obtained. Moreover, the treatment group significantly lived longer than the control mice.

HEPA1-6 tumors, however, showed no significant difference (**Figure 6F**). Moreover, the tumors of both control and treatment groups showed reduced cell viability after day 3.

Significant results were obtained in the PAN02 mouse model; however, a decreasing trend in cell viability was observed in the control mice (**Figure 6G**).

DISCUSSION

HNSCC is the seventh most common cancer worldwide, with a predicted 30% annual increase in incidence over the coming six years, highlighting the urgency of addressing this major challenge (3). OSCC stands out as the predominant subtype of HNSCC, comprising over half of all cases. Conventional treatments, including chemotherapy, immunotherapy, radiotherapy, surgery, and combinatorial therapy, have not enhanced the patient's survival rate in the last decades (4, 5). Moreover, these systemic approaches often result in profound physical and emotional side effects (9). Hence, a more local and targeted strategy that offers enhanced therapeutic efficacy and fewer adverse effects compared to existing treatments is desired. Numerous preclinical studies demonstrate promising results utilizing the HSV1-TK/GCV system to

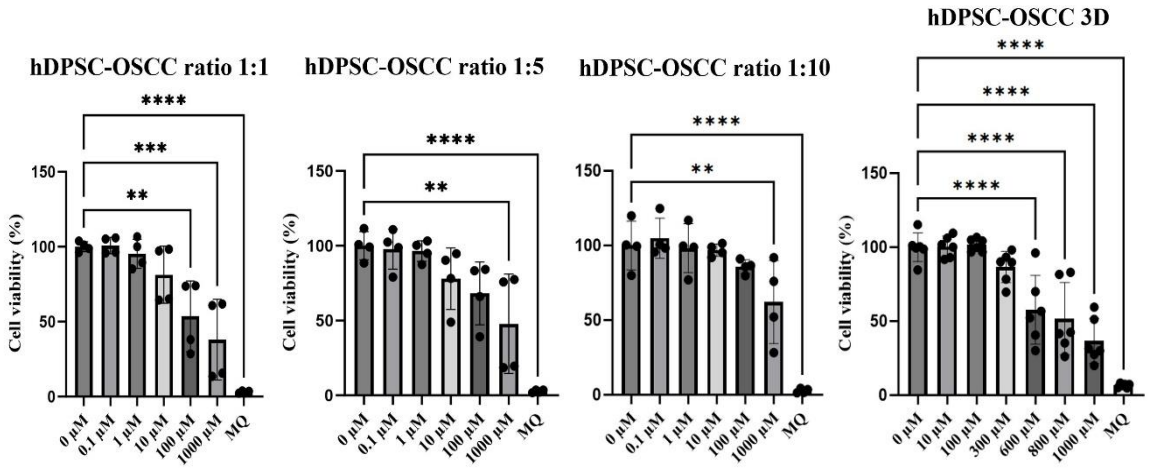

Figure 3 - Cell viability assessment of three different ratios of 2D hDPSC-OSC and 3D hDPSC-OSCC after GCV administration. The 2D (n=2) and 3D (n=3) co-cultures were treated every 2 to 3 days with five and six different GCV concentrations, respectively. The alamarBlue assay was performed after 7 and 14 days for the 2D and 3D co-cultures, respectively. A significant reduction was observed from 100 µM in the 2D culture, while the 3D culture showed a significant reduction in cell viability from 600 µM. Each data is expressed as mean ± SEM. Data were normally distributed. No outliers were observed. One-way ANOVA with Dunnett's multiple comparisons test was used. **$p \leq 0.01$, ***$p \leq 0.001$, ****$p \leq 0.0001$. *hDPSC, human Dental Pulp Stem Cells; MQ: Milli-Q; OSCC, Oral Squamous Cell Carcinoma.*

eradicate various cancer types (46-49). However, these studies employ viral vectors to deliver *HSV1-tk* to the tumor cells, raising safety concerns and restricting its clinical application (27). As a result, a safer approach, such as cell-based delivery, is of high importance. A promising strategy is the use of stem cells, which interact with tumor cells and are a potential carrier for therapeutic drugs (50, 51). Kenarkoohi *et al*. demonstrated successful transduction of murine MSC with a lentiviral vector containing *HSV1-tk* produced by human HEK293T cells for suicide gene therapy in a cervical tumor mouse model (16). Furthermore, Dührsen *et al*. demonstrated a prolonged survival rate of mice containing human glioblastoma after HSV1-TK$^+$-MSC and GCV injections (52). However, the MSC were isolated from bone marrow, involving an invasive harvest procedure that may lead to pain and risk of infection (53). Another MSC type, hDPSC, circumvents this drawback as its isolation is relatively straightforward from extracted third molars, which are medical waste products, posing no risk to the donor (37, 38). Horikawa *et al.* and Merckx *et al.* indicated that intratumoral injection of hDPSC is a promising method for delivering antitumor agents in HNSCC (36, 54). Therefore, this project proposes to use hDPSC as the cell-based delivery system for suicide gene therapy, specifically targeting OSCC in a precise manner.

The **first objective** aimed to investigate the efficacy of the HSV1-TK/GCV system in 2D and 3D co-cultures of transduced hDPSC and OSCC cells via cell viability measurements. The 2D model demonstrated a significant reduction in cell viability after administering 10 µM GCV or higher for seven days. Matuska e*t al.* observed similar results in a 2D HSV1-TK$^+$-MSC-glioblastoma co-culture (55). In contrast, the 3D model did not exhibit a similar effect after 14 days of GCV administration. This observation can be explained by the collagen hydrogel potentially obstructing the GCV, making it more difficult for the drug to reach the cells. This occurrence is absent in the 2D co-cultures, whereas the GCV is directly exposed to the cancer and stem cells. Due to the notable results of the 2D model in Figure 2, additional co-cultures were constructed with various hDPSC and OSCC ratios in Figure 3. The quantity of hDPSC was reduced compared to the cancer cells, simulating the potential future clinical application. In contrast to the previous experiment, no significant result was observed with 10 µM GCV administrations in the 2D

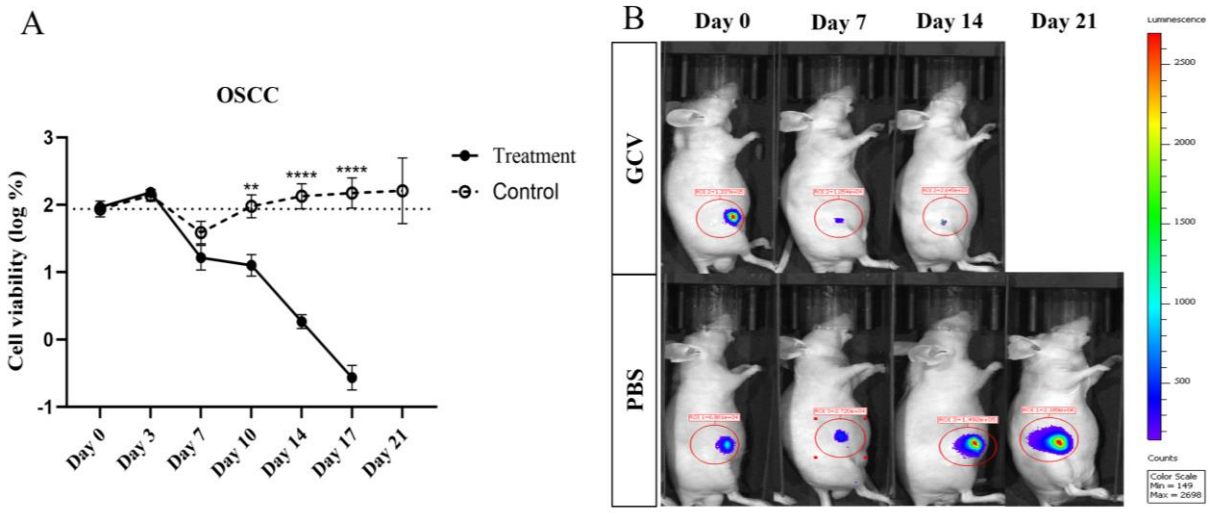

Figure 4 - Cell viability assessment of HSV1-TK$^+$-OSCC cells in a xenograft mouse model. BLI of HSV1-TK$^+$-OSCC cells after administration of daily GCV (treatment group) or PBS (control group). Cell viability **(A)** was monitored over 21 days, revealing a significant reduction in the treatment group from day 10. In contrast, the tumor viability of the control group continued to increase throughout the study. The representative images **(B)** show fluorescence measurements of one treatment mouse receiving GCV and one control mouse receiving PBS of day 0, 7, 14, and 21. No image of the treatment mouse on day 21 was obtained because no signal was observed. ROI of mouse receiving GCV: $1.337x10^5$ (day 0), $1.054x10^4$ (day 7), and $2.2645x10^3$ (day 14). ROI of mouse receiving PBS: $6.861x10^4$ (day 0), $2.720x10^4$ (day 7), $1.492x10^5$ (day 14), and $2.189x10^6$ (day 21). Each data is expressed as mean ± SEM. Data were normally distributed. No outliers were observed. Two-way ANOVA was used. **p ≤ 0.01, ****p ≤ 0.0001. *GCV, Ganciclovir; HSV1-TK$^+$-OSCC, Herpes Simplex Virus Type 1 Thymidine Kinase positive Oral Squamous Cell Carcinoma; PBS, Phosphate-Buffer Saline; ROI, Region Of Interest.*

model with an equal amount of cancer and stem cells. Furthermore, the ratios 1:5 and 1:10 of hDPSC and OSCC cells showed only a decreasing trend. However, the obtained data is based on only two sets of experiments, whereas Figure 2 includes results from seven repetitions. Therefore, additional sets of experiments must be conducted for validation. Moreover, noticeable variances between the data points in both figures are observed, further underscoring the need for additional analysis. In the 3D model of Figure 2, a notable difference in cell viability was observed between 100 µM and 1000 µM GCV. Only the latter achieved significance, indicating that further research is needed to explore the effects of intermediate concentrations. As a result, additional GCV solutions were investigated, leading to a decreased cell viability obtained from 600 µM GCV. Notably, both co-culture models exhibited decreased cell viability at 1000 µM GCV, suggesting cytotoxicity. In literature, cytotoxic effects of GCV were observed in 2D cultures of cancer and healthy cells between a concentration of 500 µM and 1000 µM (56, 57). Furthermore, our preliminary data indicated a significant cytotoxic effect of 1000 µM GCV in non-transduced 2D hDPSC-OSCC co-cultures but not in the non-transduced 3D model.

The **second objective** was to evaluate the therapeutic efficacy in a xenograft mouse model containing HSV1-TK$^+$-OSCC cells through BLI. In a systematic review of Shen *et al.*, BLI was stated as a well-established tool for preclinical assessment of tumor burden in a xenograft mouse model (58). BLI facilitates images and measures engineered viable cells in living animals in a fast, high-sensitive, and non-invasive manner (59). Nevertheless, potential limitations related to BLI need to be considered. Impairment of the detected photon emission may occur through (i) attenuation or the presence of (ii) tumor necrosis or (iii) ascites (58). First, attenuation is the absorption and scattering of light by surrounding tissue, resulting in a diminished signal detected by the BLI system. Moreover, Stollfuss *et al.* indicated an insufficient correlation between BLI and

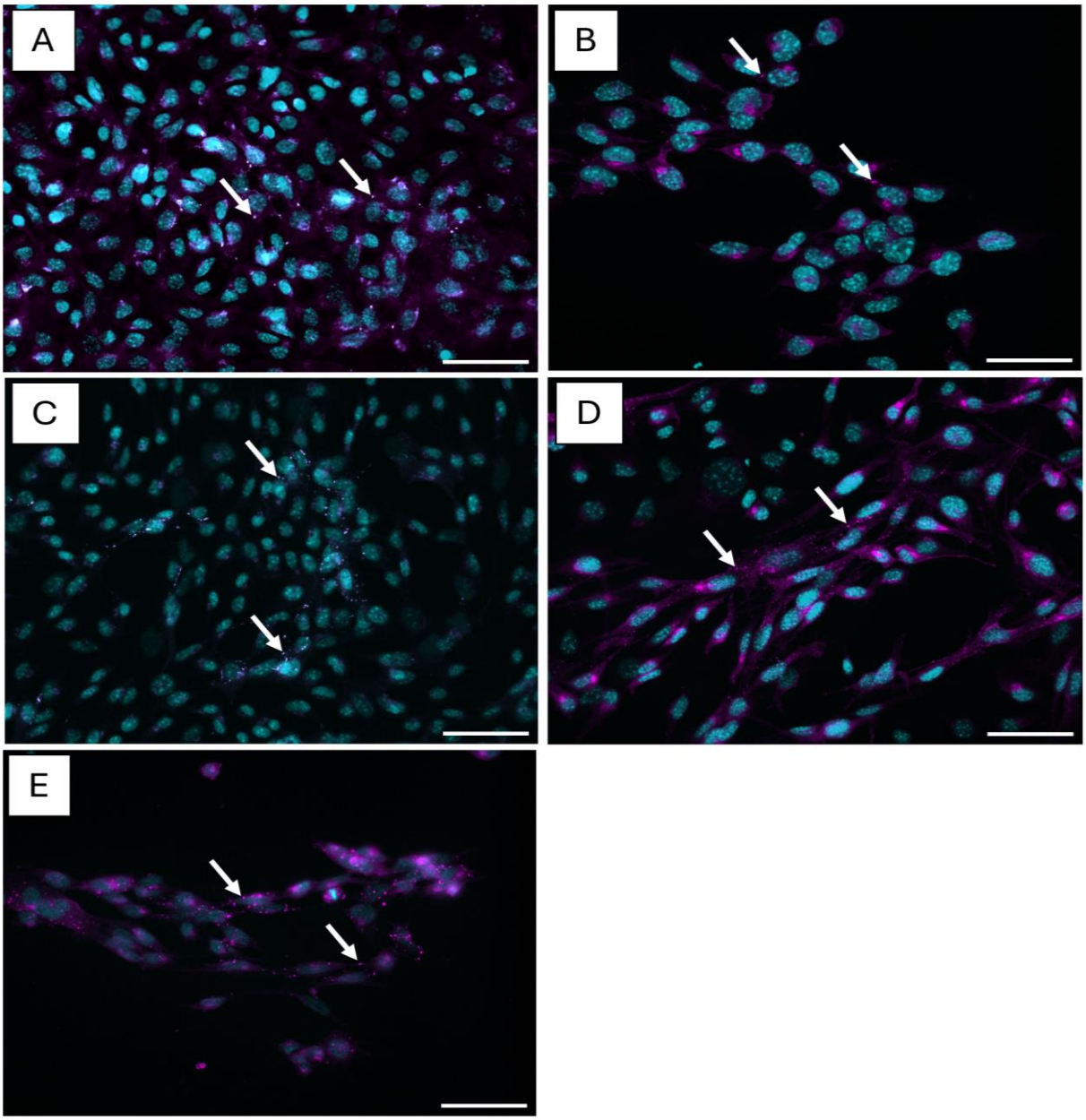

Figure 5 - Presence of gap junctions in various tumor types. Immunocytochemical (ICC) staining of Cx43 (purple dots), indicating gap junctions, shown with white arrows. The **(A)** breast (EMT-6), **(B)** lung (LL2), **(C)** colon (MC38), (**D)** pancreatic (PAN02), and **(E)** kidney (RENCA) tumor cells were obtained with the Leica DM4000 B microscope at 40x and processed with FIJI ImageJ2 software. Nuclei (blue) were stained with DAPI. Scalebars, 50 µM. *Cx43, Connexin 43.*

tumor volume in an intraperitoneal xenograft mouse model caused by the tissue between the tumor and BLI detector (60). Nevertheless, attenuation is limited in a subcutaneous xenograft model, leading to a strong correlation between BLI and tumor burden (58). Another vital factor to consider is necrosis, which was observed by Hadaschik *et al.* in a subcutaneous colon xenograft mouse model. The necrotic area of the tumor led to a decrease in overall signal intensity measured by BLI, as the transformation of D-luciferin requires viable cells (61). However, no OSCC tumor developed a necrotic area in this study. Lastly, the formation of ascites in tumors is correlated to a reduced bioluminescence signal in xenograft mouse models. However, this limitation is associated with peritoneal models rather than subcutaneous models (58). Furthermore, this proof-of-concept study only utilized male mice to minimize variations between the animals. However, gender is an important factor, as it

A

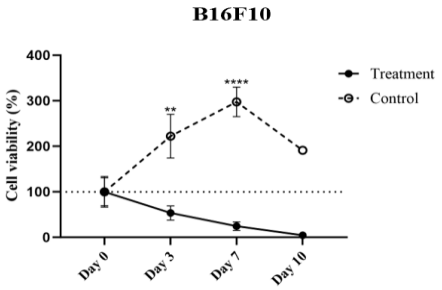
B16F10
Cell viability (%)
Treatment
Control
Day 0
Day 3
Day 7
Day 10

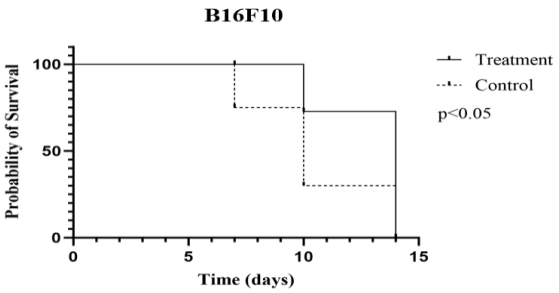
B16F10
Probability of Survival
Time (days)
Treatment
Control
p<0.05

B

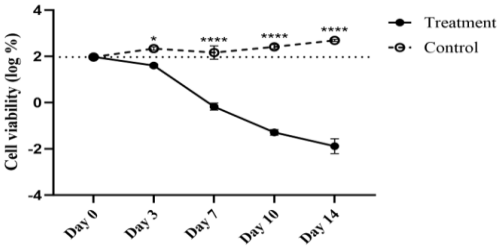
EMT6
Cell viability (log %)
Treatment
Control
Day 0
Day 3
Day 7
Day 10
Day 14

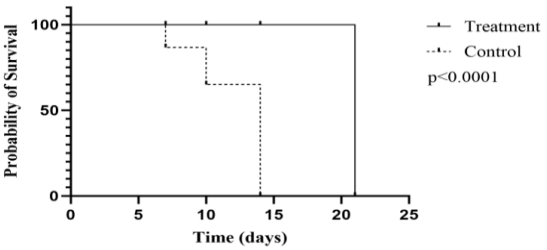
EMT6
Probability of Survival
Time (days)
Treatment
Control
p<0.0001

C

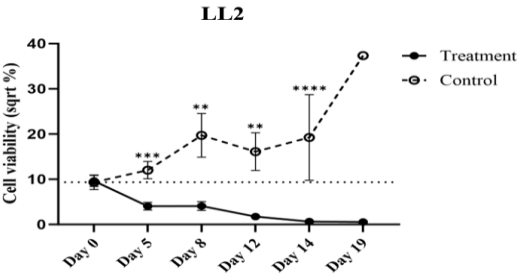
LL2
Cell viability (sqrt %)
Treatment
Control
Day 0
Day 5
Day 8
Day 12
Day 14
Day 19

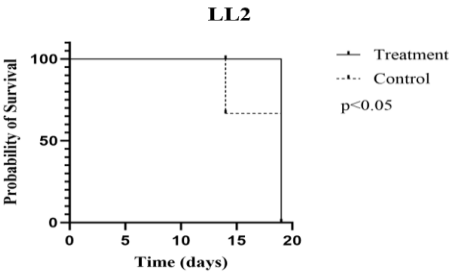
LL2
Probability of Survival
Time (days)
Treatment
Control
p<0.05

D

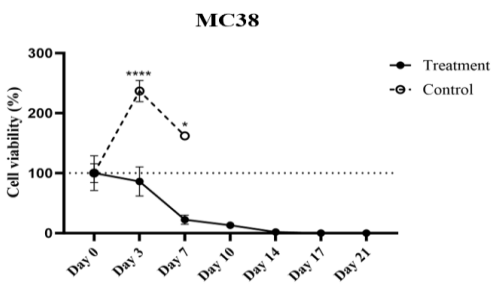
MC38
Cell viability (%)
Treatment
Control
Day 0
Day 3
Day 7
Day 10
Day 14
Day 17
Day 21

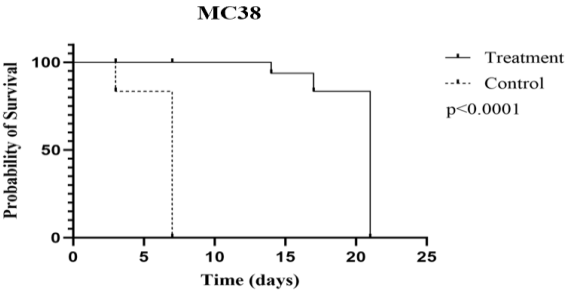
MC38
Probability of Survival
Time (days)
Treatment
Control
p<0.0001

E

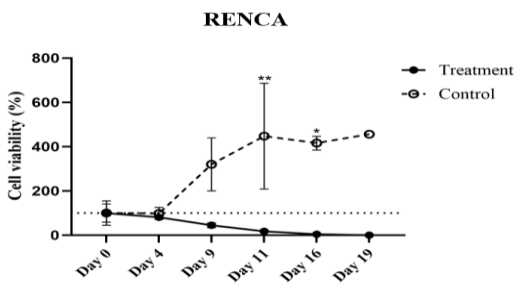
RENCA
Cell viability (%)
Treatment
Control
Day 0
Day 4
Day 9
Day 11
Day 16
Day 19

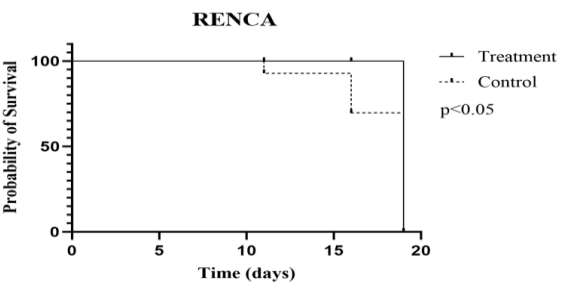
RENCA
Probability of Survival
Time (days)
Treatment
Control
p<0.05

F

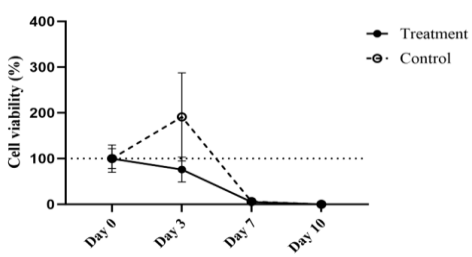
HEPA1-6
Cell viability (%)
Treatment
Control
Day 0
Day 3
Day 7
Day 10

G

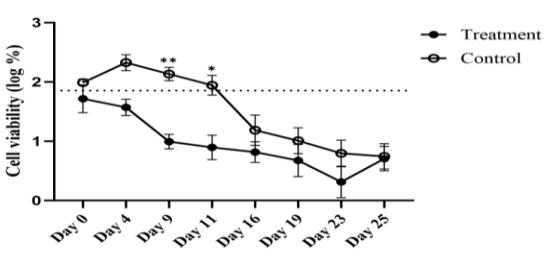
PAN02
Cell viability (log %)
Treatment
Control
Day 0
Day 4
Day 9
Day 11
Day 16
Day 19
Day 23
Day 25

Figure 6 - Cell viability assessment of various cancer cells *in vivo*. BLI of HSV1-TK$^+$-cancer cells after administration of daily GCV (treatment group) or PBS (control group). If feasible, cell viability was monitored over 19 (LL2 and RENCA), 21 (B16F10, EMT6, MC38, and HEPA1-6), or 25 days (PAN02). **(A)** The melanoma (B16F10) of the treatment group exhibited a significant reduction in cell viability on days 3 and 7, significantly affecting survival. (**B)** The mammary tumor (EMT6) showed similar results, indicating a decreased cell viability starting from day 3 upon GCV administration. All control mice reached the human endpoint by day 14. **(C)** LL2 showed a significant difference in cell viability between the two groups of mice from day 5 to day 14. The treated mice lived significantly longer compared to the control mice. **(D)** Days 3 and 7 showed a significant difference between the two groups of MC38. By day 14, the measured BLI signal was (nearly) absent in all mice receiving GCV. No BLI observations of the control group were included after day 7. **(E)** The kidney cell line (RENCA) obtained significant differences between the two groups on days 11 and 16, with significantly improved survival observed in the treatment group. **(F)** The cell viability of the liver tumors (HEPA1-6) decreased in both the treatment and control groups. No BLI measurements were obtained after day 10. **(G)** Pancreatic cancer (PAN02) showed a significant difference in cell viability between the two groups on days 9 and 11. However, both groups displayed reduced cell viability compared to day 0. Each data is expressed as mean ± SEM. Data were normally distributed. Outliers were detected and excluded. Two-way ANOVA was used for all data. *$p \leq 0.05$, **$p \leq 0.01$, ***$p \leq 0.001$, ****$p \leq 0.0001$.

may influence tumor growth and therapy efficiency. Vichaya e*t al*. observed more considerable growth of HPV-induced HNSCC in male mice compared to female mice (62). In addition, a significant response was observed in a nude female xenograft mouse model with female colon cancer cells following 5-FU treatment, which was not obtained in the male xenograft model with male colon tumors (63). In contrast, an analysis of 284 mice with five different brain tumors revealed no significant gender-based differences, suggesting that both genders are suitable for use in a xenograft mouse model (64). Another critical element is the amount of stress the mice experience, which may impact the study's findings differently in males and females. Kerr *et al.* concluded that stress could lead to significantly lower overall tumor growth in female mice compared to male mice (65). Consequently, future experiments should include both sexes to investigate potential variations. In terms of tumor volumes, relatively slow growth was observed in the mice receiving PBS throughout this study, which is a common feature of OSCC xenograft mouse models (66). Nevertheless, a significant reduction in cell viability was observed in the treatment group compared to the control mice from day 10 to day 17. No significance could be calculated for the mice receiving GCV on day 21 due to the absence of tumor cells. Moreover, a fluorescent value of zero was obtained, which is impossible to use for a logarithmic transformation. In conclusion, the BLI measurements of day 17 indicated an almost complete absence of viable tumor cells after daily GCV injections, with no tumors macroscopically visible at the end of the study.

The **third objective** was to investigate whether the HSV1-TK/GCV system has the potential to induce apoptosis of various cancer types. Therefore, the therapeutic efficacy was evaluated on breast, colon, kidney, liver, lung, pancreatic, and skin cancer. These cancer types were included due to their immense incidence and mortality. Each year, lung, colon, pancreatic, and breast cancer rank as the top four most lethal cancer types. Skin and kidney cancers are the fifth and eighth most common cancers. Furthermore, pancreatic, liver, and lung cancer all have a survival rate of less than 27%. (67). As described previously, the success of the HSV1-TK/GCV system depends on the bystander effect, which requires the presence of GJIC between adjacent cells. This requirement arises because the produced cytotoxic GCV within the genetically modified cells must be transferred into the cancer cells to induce tumor apoptosis. As mentioned before, Cx43 is the most prevalent connexin in human gap junctions and an indicator for GJIC (22, 23). Brockmeyer *et al.* showed that membrane Cx43 is upregulated in OSCC tissue compared to the tumor-free oral mucosa of the same patients. Moreover, the increased Cx43 expression is associated with a poor prognosis (22, 68). These observations highlight the relevance of our novel strategy in addressing OSCC. As previously mentioned, Van den Bosch *et al*. conducted an unpublished study in our prior research to visualize GJIC between OSCC cells. However, to determine the applicability of this

novel strategy to other tumors, the assessment of GJIC in other cancer cell types is necessary. Consequently, Cx43 was visualized in five of the seven used cancer cell lines. These results indicate that the HSV1-TK/GCV therapy holds promise in targeting various tumor types. Cx43 was successfully visualized in EMT6, LL2, MC38, PAN02, and RENCA cells. However, the expression of Cx43 indicates the presence of gap junctions rather than functional GJIC, which are formed by two hemichannels of adjacent cells (22). Additional research is necessary to confirm GJIC in the various cancer cell populations. For example, the micro-injection dye transfer assay is a well-known and suitable method showing the presence of functional gap junctions. In this technique, a non-permeable fluorescent dye can only diffuse to neighboring cells through communication channels (69). Another GJIC assessment method is the scrape loading/dye transfer (SL/DT) technique. In this method, a small monolayer of cells is intentionally scraped, causing cellular damage. Next, Lucifer Yellow dye is applied to the cells, allowing it to spread to adjacent cells when functional GJIC is present (70). In addition, flow cytometry can detect the transfer of the cytoplasmic dye Calcein-AM from MSC to cancer cells, indicating the presence of functional gap junctions (55).

The HSV1-TK/GCV system was also examined *in vivo* for multiple tumor types. Similar to the OSCC xenograft mouse model, immune-compromised mice were utilized, lacking an immune system that could potentially alter the study results. Bhuniya e*t al.* conducted lentiviral vector transduction of B16F10 and LL2 cells, which were subcutaneously injected into both immunocompetent and immunodeficient mice. As a result, reduced tumor growth was observed in mice with an intact immune system (71). Consequently, nude mice were preferred for this study to investigate the proof-of-concept. The following murine cell lines were subcutaneously injected: B16F10, EMT6, MC38, HEPA1-6, PAN02, RENCA, and LL2, representing skin, breast, colon, liver, pancreatic, kidney, and lung cancer, respectively. BLI measurements of tumors with necrotic areas were excluded due to the impaired photon emission signal (61).

On days 3 and 7, a significant difference between the treated and untreated B16F10 tumors was measured. No significant result was obtained on day 10 due to the survival of only one control mouse. Despite these promising results, all mice were sacrificed on days 7 and 10 due to the presence of large tumor volumes. This outcome appears peculiar, particularly considering the significant reduction in BLI signal after GCV administrations. Li e*t al.* stated a short-lasting expression of Fluc in transfected cancer cells with the *Fluc* gene (72). However, this study performed adenoviral transfection instead of lentiviral transduction, giving our method the advantage of long-lasting expression (25). The potential explanation stems from a flawed antibiotic selection process following lentiviral transduction. Consequently, the injected cancer population comprised cells with and without the desirable *HSV1-tk*. It is hypothesized that the transduced cells exhibited slower proliferation than unmodified cells, leading to an overgrowth of the cells lacking the vector. Moreover, due to the GCV administration, HSV1-TK$^+$-B16F10 apoptosis becomes dominant. Hence, the significant results still imply the effective killing of the HSV1-TK$^+$-B16F10 cells. Furthermore, this cell line exhibited slower growth compared to the other cell lines, as not all mice had developed measurable tumors seven days post-injection. This is a common B16F10 characteristic, as Fowlkes *et al.* subcutaneously injected $2x10^5$ B16F10 cells in mice and observed a measurable melanoma three weeks post-injection (73).

The mice containing EMT6 tumors and receiving GCV exhibited a significant reduction of cancer cell viability from day 3 to day 14. All control mice were sacrificed after the fourteenth day because of large tumor volumes. After the log transformation, the 0% cell viability on days 17 and 21 of the treatment group could not be shown in a graphical representation. Notably, only male mice were utilized in this study. Particularly for breast cancer, it would be informative to assess the therapeutic efficacy in a female EMT6 mouse model, given that over 99% of the annual incidence of breast cancer occurs in women (67).

The mice with LL2 tumors showed a significant reduction of cell viability from day 5 to day 14 after GCV administrations. No significant difference between the two groups was obtained on day 19 because only one control mouse had not met the humane endpoint. Nevertheless, despite an overall broad

variance between the control mice, 0.62% cancer cell viability was obtained in the treatment group on day 19. Additionally, a significant difference was observed in the survival curve. Alekseenko *et al.* also observed an increased survival following the administration of GCV to HSV1-TK$^+$-LL2 tumors *in vivo*. Moreover, an increasing variance in tumor volume among mice was observed over time (74). Both the corresponding research and our study injected no more than half a million cancer cells into the mice. Injecting a larger number of cells could potentially reduce variances in tumor growth, as random cancer cell death during the initial injection would have less impact on a larger cell population. However, subcutaneous injection of $5x10^7$ LL2 cells still leads to notable variances in tumor weight and volume in a xenograft mouse model (75).

The MC38 model resulted in a significant difference on the third and seventh days of the experiments. The humane endpoint was reached for all control mice on days 7 and 10. Moreover, the observed high growth rate is potentially a consequence of the transduction itself, as a significant difference in tumor growth has been reported between transduced and non-transduced MC38 tumors *in vivo.* Additionally, MC38 cells transduced with a retroviral vector lacking the suicide gene exhibited significantly lower tumor growth compared to HSV1-TK$^+$-MC38 (76). It is hypothesized that *HSV1-tk* itself is responsible for increased tumor growth, although the specific mechanism remains elusive. Moreover, the introduction of the suicide gene leads to the activation of the nuclear factor-kappa B (NF-$_K$B) pathway, leading to an increased level of cyclooxygenase-2 (COX-2), which is associated with enhanced tumor growth and resistance to apoptosis (77). Nevertheless, no photon signal was observed in all mice receiving GCV at the end of the study. Furthermore, Ishii-Morita e*t al.* investigated tumor growth using a mixture of subcutaneously introduced HSV-TK$^+$-MC38 and unmodified MC38. Administration of GCV twice daily from day 4 to day 10 following tumor injection eradicated the cancer cells by the sixth week. Consequently, the elimination of the non-transduced cancer cells potentially illustrates the occurrence of the bystander effect in the MC38 population (78). In contrast, our study observed an increased tumor volume and a reduced BLI signal in the control mice, suggesting the presence of untransduced MC38 cells (cfr. B16F10 group). The discrepancy between the two studies lies in the GCV concentration, with this study utilizing a concentration three times lower than the corresponding paper.

Mice containing RENCA xenografts and receiving GCV had significantly reduced cell viability from day 11. The humane endpoint was reached in almost all control mice on day 19, resulting in no significant result. The survival curve showed a significant difference between the two groups. However, our proof-of-concept study exclusively employed GCV administrations due to the presence of HSV1-TK$^+$-RENCA cells rather than the injection of the modified hDPSC with GCV. In contrast, Kim e*t al.* administered intravenously HSV1-TK$^+$-MSC and GCV to mice following intravenous injection of RENCA cells, which predominantly metastasized to the lungs. Moreover, improved survival of the treatment group was observed, and the modified MSC were more prominently detected in the lungs of tumor-bearing mice compared to those without. This suggests that MSC home to the tumor area (79). However, the modified MSC contained the additional *TNF-related apoptosis-inducing ligand (TRAIL),* which enhanced cancer cell apoptosis. Additionally, the MSC were derived from rat bone marrow rather than human stem cells, raising potential ethical concerns for future clinical applications. This issue does not arise with hDPSC, which are relatively easy to isolate and are obtained from clinical waste products (37, 38). Nevertheless, including a metastasis RENCA model would be informative, considering 33% of patients with renal cell cancer develop metastases (80).

Lastly, HEPA1-6 and PAN02 showed a reduction of cell viability in all animals, including mice receiving PBS. However, PAN02 presented significant differences on days 9 and 11. Literature indicates a substantial tumor growth of HEPA1-6 cells in mice, typically observed with subcutaneous injection of cell quantities ranging from $1x10^7$ to $2x10^7$ (81, 82). Despite a lower number of $5x10^6$ cells being injected in this study, a tumor still formed during the initial measurements. Furthermore, $5x10^6$ PAN02 cells should suffice, given that $5x10^5$ cancer cells have demonstrated substantial tumor growth in both male and female subcutaneous mouse models (83, 84).

Additionally, a matrigel was utilized, which should lead to enhanced cell retention and stimulate continuous tumor growth (85). Another potential factor to alter tumor growth is the immune system. $CD8^+$-T-cells can lead to apoptosis of lentiviral vector-transduced cancer cells (71, 86). However, nude mice contain a null mutation of the *forkhead transcription factor* (*FOXN1*), resulting in an unfunctional thymus. Consequently, these hairless mice have impaired T-cells (87). However, other factors of the immune system remain active. Natural autoantibodies are produced by B-lymphocytes in the absence of external antigen stimulation. Lymberi e*t al.* observed an increased level of natural autoantibodies in mice after subcutaneously injecting tumor cells (88). Another study observed reduced tumor growth in three different subcutaneously introduced pancreatic cell lines in an athymic xenograft mouse model after administering additional autoantibodies of patients (89). Furthermore, an increased production of autoantibodies induced by different cancer types has been reported in patients, including liver and pancreatic cancer. Although the mechanism remains elusive, it is theorized that these antibodies respond to newly formed antigens generated somatically by the tumor (90). However, although this phenomenon may impact tumor growth, a (almost) complete loss of tumor volume is questionable. In addition to natural autoantibodies, other parts of the immune system can potentially differ in tumor growth in our model. Murine PAN02 tumors have a higher mutational and neoantigen burden than human pancreatic tumors, resulting in the recruitment of diverse immune cells. Furthermore, HEPA1-6 and PAN02 cells originate from C57L and C57BL/6 mice (91, 92). It's plausible that the residual immune system in nude mice may mount a response against the foreign cancer cells. As far as our knowledge extends, this phenomenon remains unreported in literature. Nevertheless, NSG mouse strains may offer additional advantages as they exhibit impaired T-cells, B-cells, and natural killer (NK) cells, thereby facilitating engraftment (93). Extensive research involving larger volumes of cancer cell injections and diverse mouse strains is essential for comprehensive understanding. Additionally, *ex vivo* assessment provides further insights into underlying molecular mechanisms. Post-mortem analysis offers information on specific processes, such as cell proliferation and apoptotic events through Ki67 immunohistochemistry (IHC) and terminal deoxynucleotidyl transferase dUTP (TUNEL) analysis, respectively (89, 94). In addition, visualizing autoantibodies in tumor tissue and comparing the serum autoantibody levels of mice with and without tumors can enhance the understanding of these antibodies' involvement in tumor development and progression (89).

In the future, additional technical replicates of the 1:5 and 1:10 2D HSV1-TK^+-hDPSC-OSCC co-cultures should be produced to validate the *in vitro* findings. To further investigate the therapeutic efficacy of the GDEPT i*n vivo* and the potency of hDPSC as a vehicle of the suicide gene, the stem cells should be administered intratumorally. Moreover, the number of injections and necessary stem cell dosage needs to be evaluated. Another promising *in vivo* model is the 4-nitroquinoline-1-oxide (4NQO) rat model, which is already optimized in our research group (paper in preparation). 4NQO is a smoking-mimetic carcinogen and is administered *ad libitum*. This typical OSCC model has a high success rate in generating multiple neoplastic lesions similar to OSCC development in patients (95). Finally, potential therapy-related side effects, including toxicity, and the presence of potential metastases need to be investigated.

CONCLUSION

In conclusion, OSCC apoptosis is induced after GCV administration in 2D and 3D co-cultures with HSV1-TK^+-hDPSC. Furthermore, the cancer cell viability was significantly decreased in an OSCC xenograft mouse model after GCV administration for 21 consecutive days. Additionally, a significant reduction in subcutaneous breast, colon, kidney, lung, pancreatic, and skin tumors in mice was observed after daily GCV injections for 19, 21, or 25 days. In addition, the presence of Cx43 was visualized in breast, colon, kidney, pancreatic, and lung cancer. These results suggest that GDEPT using HSV1-TK^+-hDPSC is a promising strategy for treating OSCC and has the potential to be applied to other tumors. Nevertheless, further research is necessary to evaluate the therapeutic efficacy of the HSV1-TK^+-hDPSC/GCV system *in vivo*.

REFERENCES

1. Organization, W. H. (2024) Cancer, https://www.who.int/health-topics/cancer#tab=tab_1
2. Hanahan, D. (2022) Hallmarks of Cancer: New Dimensions Cancer Discov **12**, 31-46 10.1158/2159-8290.CD-21-1059
3. Barsouk, A., Aluru, J. S., Rawla, P., Saginala, K., andBarsouk, A. (2023) Epidemiology, Risk Factors, and Prevention of Head and Neck Squamous Cell Carcinoma Med Sci (Basel) **11**, 10.3390/medsci11020042
4. Tan, Y., Wang, Z., Xu, M., Li, B., Huang, Z., Qin, S. *et al.* (2023) Oral squamous cell carcinomas: state of the field and emerging directions Int J Oral Sci **15**, 44 10.1038/s41368-023-00249-w
5. Sun, Z., Sun, X., Chen, Z., Du, J., andWu, Y. (2022) Head and Neck Squamous Cell Carcinoma: Risk Factors, Molecular Alterations, Immunology and Peptide Vaccines Int J Pept Res Ther **28**, 19 10.1007/s10989-021-10334-5
6. Sjamsudin, E., Maulina, T., Cipta, A., Iskandarsyah, A., Hardianto, A., Nandini, M. *et al.* (2018) Assessment of oral cancer pain, anxiety, and quality of life of oral squamous cell carcinoma patients with invasive treatment procedure Oral Maxillofac Surg **22**, 83-90 10.1007/s10006-018-0672-3
7. Li, H., Zhang, Y., Xu, M., andYang, D. (2022) Current trends of targeted therapy for oral squamous cell carcinoma J Cancer Res Clin Oncol **148**, 2169-2186 10.1007/s00432-022-04028-8
8. Gyanani, V., Haley, J. C., andGoswami, R. (2021) Challenges of Current Anticancer Treatment Approaches with Focus on Liposomal Drug Delivery Systems Pharmaceuticals (Basel) **14**, 10.3390/ph14090835
9. Gondivkar, S. M., Gadbail, A. R., Sarode, S. C., Hedaoo, A., Dasgupta, S., Sharma, B. *et al.* (2021) Oral and general health-related quality of life in oral squamous cell carcinoma patients- comparative analysis of different treatment regims J Oral Biol Craniofac Res **11**, 125-131 10.1016/j.jobcr.2021.01.004
10. Minhas, S., Kashif, M., Altaf, W., Afzal, N., andNagi, A. H. (2017) Concomitant-chemoradiotherapy-associated oral lesions in patients with oral squamous-cell carcinoma Cancer Biol Med **14**, 176-182 10.20892/j.issn.2095-3941.2016.0096
11. Kolokythas, A. (2010) Long-term surgical complications in the oral cancer patient: a comprehensive review. Part I J Oral Maxillofac Res **1**, e1 10.5037/jomr.2010.1301
12. Karjoo, Z., Chen, X., andHatefi, A. (2016) Progress and problems with the use of suicide genes for targeted cancer therapy Adv Drug Deliv Rev **99**, 113-128 10.1016/j.addr.2015.05.009
13. Zhang, J., Kale, V., andChen, M. (2015) Gene-directed enzyme prodrug therapy AAPS J **17**, 102-110 10.1208/s12248-014-9675-7
14. Zarogoulidis, P., Darwiche, K., Sakkas, A., Yarmus, L., Huang, H., Li, Q. *et al.* (2013) Suicide Gene Therapy for Cancer - Current Strategies J Genet Syndr Gene Ther **4**, 10.4172/2157-7412.1000139
15. El-Sayed, A. S. A., Mohamed, N. Z., Yassin, M. A., Amer, M. M., El-Sharkawy, R., El-Sayed, N. *et al.* (2022) Microbial cytosine deaminase is a programmable anticancer prodrug mediating enzyme: antibody, and gene directed enzyme prodrug therapy Heliyon **8**, e10660 10.1016/j.heliyon.2022.e10660
16. Kenarkoohi, A., Bamdad, T., Soleimani, M., Soleimanjahi, H., Fallah, A., andFalahi, S. (2020) HSV-TK Expressing Mesenchymal Stem Cells Exert Inhibitory Effect on Cervical Cancer Model Int J Mol Cell Med **9**, 146-154 10.22088/IJMCM.BUMS.9.2.146

17. Abate-Daga, D., Garcia-Rodriguez, L., Sumoy, L., andFillat, C. (2010) Cell cycle control pathways act as conditioning factors for TK/GCV sensitivity in pancreatic cancer cells Biochim Biophys Acta **1803**, 1175-1185 10.1016/j.bbamcr.2010.06.009
18. Kokoris, M. S., andBlack, M. E. (2002) Characterization of herpes simplex virus type 1 thymidine kinase mutants engineered for improved ganciclovir or acyclovir activity Protein Sci **11**, 2267-2272 10.1110/ps.2460102
19. Gambhir, S. S., Bauer, E., Black, M. E., Liang, Q., Kokoris, M. S., Barrio, J. R. *et al.* (2000) A mutant herpes simplex virus type 1 thymidine kinase reporter gene shows improved sensitivity for imaging reporter gene expression with positron emission tomography Proc Natl Acad Sci U S A **97**, 2785-2790 10.1073/pnas.97.6.2785
20. Eissenberg, L. G., Rettig, M., Dehdashti, F., Piwnica-Worms, D., andDiPersio, J. F. (2014) Suicide genes: monitoring cells in patients with a safety switch Front Pharmacol **5**, 241 10.3389/fphar.2014.00241
21. Rossignoli, F., Hoffman, D., Atif, E., andShah, K. (2023) Developing and characterizing a two-layered safety switch for cell therapies Cancer Biol Ther **24**, 2232146 10.1080/15384047.2023.2232146
22. Lee, H. J., Cha, H. J., Jeong, H., Lee, S. N., Lee, C. W., Kim, M. *et al.* (2023) Conformational changes in the human Cx43/GJA1 gap junction channel visualized using cryo-EM Nat Commun **14**, 931 10.1038/s41467-023-36593-y
23. Yamada, A., Yoshizaki, K., Ishikawa, M., Saito, K., Chiba, Y., Fukumoto, E. *et al.* (2021) Connexin 43-Mediated Gap Junction Communication Regulates Ameloblast Differentiation via ERK1/2 Phosphorylation Front Physiol **12**, 748574 10.3389/fphys.2021.748574
24. Scheller, E. L., andKrebsbach, P. H. (2009) Gene therapy: design and prospects for craniofacial regeneration J Dent Res **88**, 585-596 10.1177/0022034509337480
25. Bulcha, J. T., Wang, Y., Ma, H., Tai, P. W. L., andGao, G. (2021) Viral vector platforms within the gene therapy landscape Signal Transduct Target Ther **6**, 53 10.1038/s41392-021-00487-6
26. Naso, M. F., Tomkowicz, B., Perry, W. L., 3rd, andStrohl, W. R. (2017) Adeno-Associated Virus (AAV) as a Vector for Gene Therapy BioDrugs **31**, 317-334 10.1007/s40259-017-0234-5
27. Lundstrom, K. (2023) Viral Vectors in Gene Therapy: Where Do We Stand in 2023? Viruses **15**, 10.3390/v15030698
28. Tiscornia, G., Singer, O., andVerma, I. M. (2006) Production and purification of lentiviral vectors Nat Protoc **1**, 241-245 10.1038/nprot.2006.37
29. Yahya, E. B., andAlqadhi, A. M. (2021) Recent trends in cancer therapy: A review on the current state of gene delivery Life Sci **269**, 119087 10.1016/j.lfs.2021.119087
30. Sung, Y. K., andKim, S. W. (2019) Recent Advances in the Development of Bio-Reducible Polymers for Efficient Cancer Gene Delivery Systems Cancer Med J **2**, 6-13, https://www.ncbi.nlm.nih.gov/pubmed/31032485
31. Mohit, E., andRafati, S. (2013) Biological delivery approaches for gene therapy: strategies to potentiate efficacy and enhance specificity Mol Immunol **56**, 599-611 10.1016/j.molimm.2013.06.005
32. Bashor, C. J., Hilton, I. B., Bandukwala, H., Smith, D. M., andVeiseh, O. (2022) Engineering the next generation of cell-based therapeutics Nat Rev Drug Discov **21**, 655-675 10.1038/s41573-022-00476-6

33. Attia, N., Mashal, M., Puras, G., andPedraz, J. L. (2021) Mesenchymal Stem Cells as a Gene Delivery Tool: Promise, Problems, and Prospects Pharmaceutics **13**, 10.3390/pharmaceutics13060843
34. Reagan, M. R., andKaplan, D. L. (2011) Concise review: Mesenchymal stem cell tumor-homing: detection methods in disease model systems Stem Cells **29**, 920-927 10.1002/stem.645
35. Zachar, L., Bacenkova, D., andRosocha, J. (2016) Activation, homing, and role of the mesenchymal stem cells in the inflammatory environment J Inflamm Res **9**, 231-240 10.2147/JIR.S121994
36. Merckx, G., Lo Monaco, M., Lambrichts, I., Himmelreich, U., Bronckaers, A., andWolfs, E. (2021) Safety and Homing of Human Dental Pulp Stromal Cells in Head and Neck Cancer Stem Cell Rev Rep **17**, 1619-1634 10.1007/s12015-021-10159-1
37. Hilkens, P., Gervois, P., Fanton, Y., Vanormelingen, J., Martens, W., Struys, T. *et al.* (2013) Effect of isolation methodology on stem cell properties and multilineage differentiation potential of human dental pulp stem cells Cell Tissue Res **353**, 65-78 10.1007/s00441-013-1630-x
38. Wang, W., Yan, M., Aarabi, G., Peters, U., Freytag, M., Gosau, M. *et al.* (2022) Cultivation of Cryopreserved Human Dental Pulp Stem Cells-A New Approach to Maintaining Dental Pulp Tissue Int J Mol Sci **23**, 10.3390/ijms231911485
39. Sadikot, R. T., andBlackwell, T. S. (2005) Bioluminescence imaging Proc Am Thorac Soc **2**, 537-540, 511-532 10.1513/pats.200507-067DS
40. Becker, M., andZaidi, H. (2014) Imaging in head and neck squamous cell carcinoma: the potential role of PET/MRI Br J Radiol **87**, 20130677 10.1259/bjr.20130677
41. Berger, A. (2002) Magnetic resonance imaging BMJ **324**, 35 10.1136/bmj.324.7328.35
42. Ribeiro, F. M., Correia, P. M. M., Santos, A. C., andVeloso, J. (2022) A guideline proposal for mice preparation and care in (18)F-FDG PET imaging EJNMMI Res **12**, 49 10.1186/s13550-022-00921-y
43. Burglin, S. A., Hess, S., Hoilund-Carlsen, P. F., andGerke, O. (2017) 18F-FDG PET/CT for detection of the primary tumor in adults with extracervical metastases from cancer of unknown primary: A systematic review and meta-analysis Medicine (Baltimore) **96**, e6713 10.1097/MD.0000000000006713
44. Omami, G., Tamimi, D., andBranstetter, B. F. (2014) Basic principles and applications of (18)F-FDG-PET/CT in oral and maxillofacial imaging: A pictorial essay Imaging Sci Dent **44**, 325-332 10.5624/isd.2014.44.4.325
45. Saldin, L. T., Cramer, M. C., Velankar, S. S., White, L. J., andBadylak, S. F. (2017) Extracellular matrix hydrogels from decellularized tissues: Structure and function Acta Biomater **49**, 1-15 10.1016/j.actbio.2016.11.068
46. Poorghobadi, S., Hosseini, S. Y., Sadat, S. M., Abdoli, A., Irani, S., andBaesi, K. (2024) The Combinatorial Effect of Ad-IL-24 and Ad-HSV-tk/GCV on Tumor Size, Autophagy, and UPR Mechanisms in Multiple Myeloma Mouse Model Biochem Genet 10.1007/s10528-024-10671-2
47. Lv, Y. F., Zhang, H., Cui, Z., Ma, C. J., Li, Y. L., Lu, H. *et al.* (2023) Gene delivery to breast cancer by incorporated EpCAM targeted DARPins into AAV2 BMC Cancer **23**, 1220 10.1186/s12885-023-11705-5
48. Tseng, J. C., Zanzonico, P. B., Levin, B., Finn, R., Larson, S. M., andMeruelo, D. (2006) Tumor-specific in vivo transfection with HSV-1 thymidine kinase gene using a Sindbis

viral vector as a basis for prodrug ganciclovir activation and PET J Nucl Med **47**, 1136-1143, https://www.ncbi.nlm.nih.gov/pubmed/16818948

49. Nasu, Y., Bangma, C. H., Hull, G. W., Yang, G., Wang, J., Shimura, S. *et al.* (2001) Combination gene therapy with adenoviral vector-mediated HSV-tk+GCV and IL-12 in an orthotopic mouse model for prostate cancer Prostate Cancer Prostatic Dis **4**, 44-55 10.1038/sj.pcan.4500494
50. Hass, R. (2020) Role of MSC in the Tumor Microenvironment Cancers (Basel) **12**, 10.3390/cancers12082107
51. Lv, F. J., Tuan, R. S., Cheung, K. M., andLeung, V. Y. (2014) Concise review: the surface markers and identity of human mesenchymal stem cells Stem Cells **32**, 1408-1419 10.1002/stem.1681
52. Duhrsen, L., Hartfuss, S., Hirsch, D., Geiger, S., Maire, C. L., Sedlacik, J. *et al.* (2019) Preclinical analysis of human mesenchymal stem cells: tumor tropism and therapeutic efficiency of local HSV-TK suicide gene therapy in glioblastoma Oncotarget **10**, 6049-6061 10.18632/oncotarget.27071
53. Mastrolia, I., Foppiani, E. M., Murgia, A., Candini, O., Samarelli, A. V., Grisendi, G. *et al.* (2019) Challenges in Clinical Development of Mesenchymal Stromal/Stem Cells: Concise Review Stem Cells Transl Med **8**, 1135-1148 10.1002/sctm.19-0044
54. Horikawa, M., Koizumi, S., Oishi, T., Yamamoto, T., Ikeno, M., Ito, M. *et al.* (2023) Potent bystander effect and tumor tropism in suicide gene therapy using stem cells from human exfoliated deciduous teeth Cancer Gene Ther **30**, 85-95 10.1038/s41417-022-00527-5
55. Matuskova, M., Hlubinova, K., Pastorakova, A., Hunakova, L., Altanerova, V., Altaner, C. *et al.* (2010) HSV-tk expressing mesenchymal stem cells exert bystander effect on human glioblastoma cells Cancer Lett **290**, 58-67 10.1016/j.canlet.2009.08.028
56. He, X. L., Guo, X. J., Qian, G. S., He, X. H., Huang, G. J., Chen, W. Z. *et al.* (2001) Killing effects of ganciclovir on human pulmonary adenocarcinoma cell A549 transduced with HSV1-TK gene in vitro and in vivo Acta Pharmacol Sin **22**, 901-906, https://www.ncbi.nlm.nih.gov/pubmed/11749772
57. Wang, J., Lu, X. X., Chen, D. Z., Li, S. F., andZhang, L. S. (2004) Herpes simplex virus thymidine kinase and ganciclovir suicide gene therapy for human pancreatic cancer World J Gastroenterol **10**, 400-403 10.3748/wjg.v10.i3.400
58. Shen, Y. T., Asthana, R., Peeters, C., Allen, C., DeAngelis, C., andPiquette-Miller, M. (2020) Potential Limitations of Bioluminescent Xenograft Mouse Models: A Systematic Review J Pharm Pharm Sci **23**, 177-199 10.18433/jpps30870
59. Ramasawmy, R., Johnson, S. P., Roberts, T. A., Stuckey, D. J., David, A. L., Pedley, R. B. *et al.* (2016) Monitoring the Growth of an Orthotopic Tumour Xenograft Model: Multi-Modal Imaging Assessment with Benchtop MRI (1T), High-Field MRI (9.4T), Ultrasound and Bioluminescence PLoS One **11**, e0156162 10.1371/journal.pone.0156162
60. Stollfuss, J., Landvogt, N., Abenstein, M., Ziegler, S., Schwaiger, M., Senekowitsch-Schmidtke, R. *et al.* (2015) Non-invasive imaging of implanted peritoneal carcinomatosis in mice using PET and bioluminescence imaging EJNMMI Res **5**, 125 10.1186/s13550-015-0125-z
61. Inoue, Y., Sheng, F., Kiryu, S., Watanabe, M., Ratanakanit, H., Izawa, K. *et al.* (2011) Gaussia luciferase for bioluminescence tumor monitoring in comparison with firefly luciferase Mol Imaging **10**, 377-385 10.2310/7290.2010.00057

62. Vichaya, E. G., Ford, B. G., Moltenkine, J. M., Taniguchi, C. M., Phillip West, A., andDantzer, R. (2021) Sex differences in the behavioral and immune responses of mice to tumor growth and cancer therapy Brain Behav Immun **98**, 161-172 10.1016/j.bbi.2021.08.225
63. Lim, H., Kim, S. Y., Lee, E., Lee, S., Oh, S., Jung, J. *et al.* (2019) Sex-Dependent Adverse Drug Reactions to 5-Fluorouracil in Colorectal Cancer Biol Pharm Bull **42**, 594-600 10.1248/bpb.b18-00707
64. Qi, L., Kogiso, M., Du, Y., Zhang, H., Braun, F. K., Huang, Y. *et al.* (2020) Impact of SCID mouse gender on tumorigenicity, xenograft growth and drug-response in a large panel of orthotopic PDX models of pediatric brain tumors Cancer Lett **493**, 197-206 10.1016/j.canlet.2020.08.035
65. Kerr, L. R., Wilkinson, D. A., Emerman, J. T., andWeinberg, J. (1999) Interactive effects of psychosocial stressors and gender on mouse mammary tumor growth Physiol Behav **66**, 277-284 10.1016/s0031-9384(98)00296-0
66. Hussein, I. T., Miguel, R. N., Tiley, L. S., andField, H. J. (2008) Substrate specificity and molecular modelling of the feline herpesvirus-1 thymidine kinase Arch Virol **153**, 495-505 10.1007/s00705-007-0021-6
67. INSITUTE, N. C. (2024) Cancer Stat Facts: Common Cancer Sites
68. Brockmeyer, P., Hemmerlein, B., Jung, K., Fialka, F., Brodmann, T., Gruber, R. M. *et al.* (2016) Connexin subtype expression during oral carcinogenesis: A pilot study in patients with oral squamous cell carcinoma Mol Clin Oncol **4**, 298-302 10.3892/mco.2015.685
69. Trosko, J. E., Chang, C. C., Wilson, M. R., Upham, B., Hayashi, T., andWade, M. (2000) Gap junctions and the regulation of cellular functions of stem cells during development and differentiation Methods **20**, 245-264 10.1006/meth.1999.0941
70. Babica, P., Sovadinova, I., andUpham, B. L. (2016) Scrape Loading/Dye Transfer Assay Methods Mol Biol **1437**, 133-144 10.1007/978-1-4939-3664-9_9
71. Bhuniya, A., Pattarayan, D., andYang, D. (2022) Lentiviral vector transduction provides nonspecific immunogenicity for syngeneic tumor models Mol Carcinog **61**, 1073-1081 10.1002/mc.23467
72. Li, Y., Liu, M., Cui, J., Yang, K., Zhao, L., Gong, M. *et al.* (2018) Hepa1-6-FLuc cell line with the stable expression of firefly luciferase retains its primary properties with promising bioluminescence imaging ability Oncol Lett **15**, 6203-6210 10.3892/ol.2018.8132
73. Fowlkes, N., Clemons, K., Rider, P. J., Subramanian, R., Wakamatsu, N., Langohr, I. *et al.* (2019) Factors Affecting Growth Kinetics and Spontaneous Metastasis in the B16F10 Syngeneic Murine Melanoma Model Comp Med **69**, 48-54 10.30802/AALAS-CM-18-000036
74. De Palma, M., Venneri, M. A., Roca, C., andNaldini, L. (2003) Targeting exogenous genes to tumor angiogenesis by transplantation of genetically modified hematopoietic stem cells Nat Med **9**, 789-795 10.1038/nm871
75. Xue, Q., Liu, Z., Feng, Z., Xu, Y., Zuo, W., Wang, Q. *et al.* (2020) Penfluridol: An antipsychotic agent suppresses lung cancer cell growth and metastasis by inducing G0/G1 arrest and apoptosis Biomed Pharmacother **121**, 109598 10.1016/j.biopha.2019.109598
76. Konson, A., Ben-Kasus, T., Mahajna, J. A., Danon, A., Rimon, G., andAgbaria, R. (2004) Herpes simplex virus thymidine kinase gene transduction enhances tumor growth rate and cyclooxygenase-2 expression in murine colon cancer cells Cancer Gene Ther **11**, 830-840 10.1038/sj.cgt.7700768

77. Konson, A., Mahajna, J. A., Danon, A., Rimon, G., andAgbaria, R. (2006) The involvement of nuclear factor-kappa B in cyclooxygenase-2 overexpression in murine colon cancer cells transduced with herpes simplex virus thymidine kinase gene Cancer Gene Ther **13**, 1093-1104 10.1038/sj.cgt.7700983
78. Ishii-Morita, H., Agbaria, R., Mullen, C. A., Hirano, H., Koeplin, D. A., Ram, Z. *et al.* (1997) Mechanism of 'bystander effect' killing in the herpes simplex thymidine kinase gene therapy model of cancer treatment Gene Ther **4**, 244-251 10.1038/sj.gt.3300379
79. Kim, S. W., Kim, S. J., Park, S. H., Yang, H. G., Kang, M. C., Choi, Y. W. *et al.* (2013) Complete regression of metastatic renal cell carcinoma by multiple injections of engineered mesenchymal stem cells expressing dodecameric TRAIL and HSV-TK Clin Cancer Res **19**, 415-427 10.1158/1078-0432.CCR-12-1568
80. Flanigan, R. C., Campbell, S. C., Clark, J. I., andPicken, M. M. (2003) Metastatic renal cell carcinoma Curr Treat Options Oncol **4**, 385-390 10.1007/s11864-003-0039-2
81. Han, Z., Yang, D., Trivett, A., andOppenheim, J. J. (2017) Therapeutic vaccine to cure large mouse hepatocellular carcinomas Oncotarget **8**, 52061-52071 10.18632/oncotarget.19367
82. Zhou, B., Yan, J., Guo, L., Zhang, B., Liu, S., Yu, M. *et al.* (2020) Hepatoma cell-intrinsic TLR9 activation induces immune escape through PD-L1 upregulation in hepatocellular carcinoma Theranostics **10**, 6530-6543 10.7150/thno.44417
83. Krzykawski, M. P., Krzykawska-Serda, M., Jasinska, K., andMarcinkiewicz, J. (2015) Pan_02 murine pancreatic cancer model Folia Med Cracov **55**, 15-24, https://www.ncbi.nlm.nih.gov/pubmed/26774804
84. Yan, Y., Rubinchik, S., Wood, A. L., Gillanders, W. E., Dong, J. Y., Watson, D. K. *et al.* (2006) Bystander effect contributes to the antitumor efficacy of CaSm antisense gene therapy in a preclinical model of advanced pancreatic cancer Mol Ther **13**, 357-365 10.1016/j.ymthe.2005.06.485
85. Katsuta, E., DeMasi, S. C., Terracina, K. P., Spiegel, S., Phan, G. Q., Bear, H. D. *et al.* (2016) Modified breast cancer model for preclinical immunotherapy studies J Surg Res **204**, 467-474 10.1016/j.jss.2016.06.003
86. Schwartz-Albiez, R., Monteiro, R. C., Rodriguez, M., Binder, C. J., andShoenfeld, Y. (2009) Natural antibodies, intravenous immunoglobulin and their role in autoimmunity, cancer and inflammation Clin Exp Immunol **158 Suppl 1**, 43-50 10.1111/j.1365-2249.2009.04026.x
87. Vaidya, H. J., Briones Leon, A., andBlackburn, C. C. (2016) FOXN1 in thymus organogenesis and development Eur J Immunol **46**, 1826-1837 10.1002/eji.201545814
88. Lymberi, P., Blancher, A., Calvas, P., andAvrameas, S. (1989) Natural autoantibodies in nude and normal outbred (Swiss) and inbred (BALB/c) mice J Autoimmun **2**, 283-295 10.1016/0896-8411(89)90270-9
89. Gardner-Thorpe, J., Ito, H., Ashley, S. W., andWhang, E. E. (2003) Autoantibody-mediated inhibition of pancreatic cancer cell growth in an athymic (nude) mouse model Pancreas **27**, 180-189 10.1097/00006676-200308000-00012
90. de Jonge, H., Iamele, L., Maggi, M., Pessino, G., andScotti, C. (2021) Anti-Cancer Auto-Antibodies: Roles, Applications and Open Issues Cancers (Basel) **13**, 10.3390/cancers13040813

91. Pham, T. N. D., Shields, M. A., Spaulding, C., Principe, D. R., Li, B., Underwood, P. W. *et al.* (2021) Preclinical Models of Pancreatic Ductal Adenocarcinoma and Their Utility in Immunotherapy Studies Cancers (Basel) **13**, 10.3390/cancers13030440
92. Huu Hoang, T., Sato-Matsubara, M., Yuasa, H., Matsubara, T., Thuy, L. T. T., Ikenaga, H. *et al.* (2022) Cancer cells produce liver metastasis via gap formation in sinusoidal endothelial cells through proinflammatory paracrine mechanisms Sci Adv **8**, eabo5525 10.1126/sciadv.abo5525
93. Kitsera, M., Brunetti, J. E., andRodriguez, E. (2023) Recent Developments in NSG and NRG Humanized Mouse Models for Their Use in Viral and Immune Research Viruses **15**, 10.3390/v15020478
94. Roife, D., Dai, B., Kang, Y., Perez, M. V. R., Pratt, M., Li, X. *et al.* (2016) Ex Vivo Testing of Patient-Derived Xenografts Mirrors the Clinical Outcome of Patients with Pancreatic Ductal Adenocarcinoma Clin Cancer Res **22**, 6021-6030 10.1158/1078-0432.CCR-15-2936
95. Chaves, P., Garrido, M., Oliver, J., Perez-Ruiz, E., Barragan, I., andRueda-Dominguez, A. (2023) Preclinical models in head and neck squamous cell carcinoma Br J Cancer **128**, 1819-1827 10.1038/s41416-023-02186-1

Acknowledgements – T. Raps acknowledges the University of Hasselt for his senior internship. Special thanks to Prof. dr. Esther Wolfs for giving me the opportunity to perform my senior internship and deliver this exciting research topic. Deep gratitude goes to Miss Jolien Van den Bosch for her invaluable guidance and wisdom. I am grateful to have the experience of learning various lab techniques during my internship and for Miss Jolien Van den Bosch's assistance in enhancing my writing skills. I would also like to thank all members of the FIERCE and LISSA research group for providing additional assistance and knowledge during my internship. Moreover, a special thanks to Mrs. Nuran Caz for providing further insights into head and neck cancer research. The research was funded by the Research Foundation Flanders (FWO, Vlaanderen).

Author contributions – Prof. dr. E.W. designed the research. J.V.D.B. supervised the study. J.V.D.B., N.C., and T.R. were responsible for the experiments. J.V.D.B. and T.R. performed data analysis. This paper was written by T.R. and reviewed by J.V.D.B.

This text was grammatically supported by GenAI.